

# 3D structural complexity analysis of cerebellum in Chiari malformation type I

Engin Akar<sup>1</sup> · Sadık Kara<sup>2</sup> · Hidayet Akdemir<sup>3</sup> · Adem Kırış<sup>4</sup>

Received: 8 December 2015 / Accepted: 21 May 2017 / Published online: 7 June 2017  
© International Federation for Medical and Biological Engineering 2017

**Abstract** Chiari malformation type I (CM-I), described by a descent of the cerebellar tonsils, is assumed to be a neurological developmental disorder. The aim of the present study was to investigate morphological variance in cerebellar sub-structures, including gray matter (GM), white matter (WM), and cerebrospinal fluid (CSF), using magnetic resonance (MR) images with three-dimensional (3D) fractal dimension (FD) analysis in patients with CM-I. MRI data of 16 patients and 15 control subjects were obtained, and structural complexity analyses were performed using a box-counting FD algorithm. Results showed that patients with CM-I had significantly reduced FD values for WM and CSF in comparison with controls, and statistically significant differences in cerebellar GM and CSF volumes between patients and controls were found. Moreover, a significant difference was not found between the WM volumes. This may suggest that there are changes in structural complexity in WM even when its volume is unaffected. We conclude that the findings of this preliminary study indicate the possibility of using FD analysis to understand the pathophysiology of CM-I in patients.

**Keywords** Chiari malformation · Magnetic resonance imaging · Fractal dimension · Box-counting

✉ Engin Akar  
enginakar@gmail.com

<sup>1</sup> Independent Researcher, Adnan Kahveci Mh. Konak Cd., Beyaz İnci Evleri B Blok No:19, 34528 Beylikdüzü, Istanbul, Turkey

<sup>2</sup> Independent Researcher, Istanbul, Turkey

<sup>3</sup> Department of Neurosurgery, Medicana International Hospital, Istanbul, Turkey

<sup>4</sup> Department of Radiology, Mehmet Akif Ersoy Cardio-Thoracic Surgery Training and Research Hospital, Istanbul, Turkey

## 1 Introduction

Chiari malformation type I (CM-I) is an important structural neurological disorder that is characterized by a descent of the cerebellar tonsils, which are rounded lobule-like structures that are present under each hemisphere of the cerebellum, into the cervical spinal canal through the foramen magnum, a large hole in the base of the skull [1]. This serious pathological condition was first described by Professor Hans Chiari in 1891 [2]. According to a radiological point of view, it is specified as tonsillar descent of at least 5 mm below the foramen magnum [3]. In this condition, other hindbrain regions, such as the fourth ventricle and the brainstem, keep their normal positions; however, they may be slightly deformed or reduced in size. Syringomyelia, which can be defined as the abnormal dilatation of spinal canal creating a small cavity that can be involved in the collection of cerebrospinal fluid (CSF), is an associated condition and may be observed in most Chiari patients [4].

Various conditions may trigger the formation of Chiari syndrome. Originally, it was considered to be caused by long-lasting hydrocephalus, a condition characterized by abnormal accumulation of CSF in the brain [5]. Currently, it is thought that several groups of conditions and disorders may lead to CM-I. One cause for CM-I may be changes in the equilibrium of intracranial pressure due to altered CSF circulation dynamics [1]. Another cause may be incomplete development of occipital bones and small posterior fossa dimensions, leading to an overcrowding of cerebellum [6–11]. Nevertheless, the natural history and the actual pathogenesis of this disorder are still uncertain [12, 13].

Several symptoms with various degrees of severity can be observed in patients with Chiari. Severe headaches in the back of the head, which can be triggered by Valsalva maneuvers such as coughing, sneezing, and laughing, are the most

frequent symptom of the disorder. Pain in the neck and shoulders is another common condition [14, 15]. Moreover, patients may have a group of secondary symptoms, including dysarthria, a motor speech disorder that disrupts speech quality [16]; sleep apnea [17, 18]; airway abnormalities, such as vocal cord impairment and aspiration [19, 20]; nystagmus, a neurologic condition that involves repetitive, rapid involuntary eye movements that lead to limited vision [21]; and balance and gait problems [22]. On the other hand, patients with CM-I may be asymptomatic [23], complicating the determination of the exact prevalence of the disorder, which is estimated at 0.1–0.5% [24]. An important characteristic related to this disorder is that a wide variety of its symptoms may cause misdiagnoses with other neurological diseases, such as fibromyalgia, multiple sclerosis (MS), and migraine [12]. One reason for such situations may be a lack of diagnostic tests that associate the symptoms of CM-I with its anatomical condition [16].

The most appropriate modality for the diagnosis of CM-I is magnetic resonance imaging (MRI) because midline sagittal MR images provide a proper viewpoint for monitoring tonsillar herniation [25]. Other additional diagnostic methods that are used for the identification of Chiari include computed tomography (CT) and neurological tests [26]. Furthermore, phase-contrast (PC) cine MRI, which can be used for the evaluation of CSF flow characteristics, is another type of examination that can be employed for diagnostic purposes [12, 27, 28]. Moreover, planning a successful treatment methodology that is dependent on the correct diagnosis of Chiari is another important consideration for this anomaly. The only therapeutic method available is a surgical operation called posterior fossa decompression (PFD) [29]. However, different surgical methods may be preferred because there has been strong controversy about the pathophysiology of this disorder [16]. There are neurosurgeons who consider CSF flow blockage to be the main reason for Chiari symptoms and try to restore CSF flow as a primary goal [30, 31]. Conversely, other surgeons consider the small size of the posterior cranial fossa (PCF) to be the major source of Chiari symptomatology and strive to enlarge the PCF.

The majority of previous studies that have investigated the neurological features of CM-I involved morphological assessment of hindbrain structures, including the cerebellum, brainstem, and fourth ventricle [6, 8–10, 32, 33]. In general, the morphological properties of PCF have been evaluated in sagittal MRI slices, and several linear, volumetric analyses have been performed. A typical morphological measurement that is taken is the length of the cerebellar tonsils, which can be calculated by measuring the distance between the tips of the tonsils and a line drawn from the basion to the opisthion, the midpoints on the anterior and posterior borders of the foramen magnum, respectively. Another common measurement is the length of the supraocciput, which is the distance between the opisthion and the center of the internal occipital protuberance

[6]. Other measurements include the length of the clivus, the distance between the basion, and the top of the dorsum sellae, a region of bone in the middle of the skull towards the front, and the slope of the cerebellar tentorium, a part of the brain layer that separates the occipital brain lobes and the cerebellum [6]. In addition to linear evaluations, total volumes of the brain, PCF and CSF spaces have also been calculated for volumetric assessment of the Chiari anomaly [6, 8–10, 32, 33]. On the other hand, some additional studies have made efforts to investigate CSF flow characteristics for the purpose of determining the relation between CSF flow patterns and the severity of CM-I symptoms [30, 31, 34].

Fractal dimension (FD) analysis is a widely used method in neuroscience for the quantitative measurement of morphological complexity [35–50]. This method produces a single numerical index by processing the details of structural patterns in complex objects [35–37]. It has been suggested that FD analysis may be employed to evaluate the morphology of brain cortices in patients with neurological disorders [38]. Furthermore, it has been proposed that functional and structural variations in neural system complexity during brain development or degeneration processes may be quantified by FD analysis [36, 39–41]. Additionally, this technique has been implemented in many studies related to image analysis of neurological disorders, including MS [36, 42], obsessive-compulsive disorder [35], medulloblastoma [38], schizophrenia [43, 44], tumor detection [45, 46], age-related micro-structural white matter (WM) changes [47], epilepsy [48], multiple system atrophy [37] Alzheimer's disease [49], stroke [50], and aging [51]. These previous studies [36–40, 42, 43] have also demonstrated that fractal approaches are suitable for performing morphological analyses of cerebral or cerebellar sub-structures involving white matter (WM), gray matter (GM), and WM tracts.

Although the majority of attention has been paid to morphological analyses of MR images in CM-I patients, there exists limited knowledge about the pathophysiology of the disorder and its underlying mechanisms related to cerebellar tissues. According to our hypothesis, the physical conditions that characterize the CM-I anomaly, such as tonsillar descent and overcrowding of cerebellum, may result in variations in the morphological complexities of cerebellar sub-structures such as GM, WM, and CSF. Since an FD value is a suitable numerical descriptor for morphological complexity of brain tissues and has been widely investigated in different neurological disorders, this methodology has been chosen to assess cerebellar complexity in patients with CM-I. Therefore in our recent study [52], we have performed a two-dimensional (2D) FD analysis to identify the morphological variations in cerebellum using a single midline sagittal brain MRI slice. Because, a three-dimensional (3D) calculation of FD gives a more accurate and comprehensive information about the complexity of these structures, in the present research, by

extending our previous study [52], a 3D volumetric FD analysis was carried out for morphological investigation of WM, GM and surrounding CSF spaces around cerebellum. To the best knowledge of the authors, this is the first study to apply 3D FD analysis to inspect the structural complexity of cerebella in patients with CM-I. The primary goal of this study was to examine morphological characteristics of cerebellar sub-tissues in Chiari patients. Secondly, this study aimed to compute correlations between the complexity values of cerebellar WM, GM, and CSF and the volumes of these tissues for both patients and controls. A further purpose of the present study was to compute correlations between FD values and herniation sizes of cerebellar tonsils in patients. Overall, we believe that the present study may contribute to the redefinition of the anomaly and to assist in the diagnosis, treatment, and management of patients.

## 2 Materials and methods

### 2.1 Patients and MR acquisition

MR images were obtained from databases of the radiology departments of two hospitals: Mehmet Akif Ersoy Cardio-Thoracic Surgery Training and Research Hospital and Medicana International Hospital, Istanbul. Brain images of 16 healthy subjects (5 males and 11 females, 16–50 years age range) and 15 CM-I patients (5 males and 10 females, 16–55 years age range) were selected from already existing MRI records at the mentioned hospitals, which were taken in the period between 2013 and 2015. Therefore, the present study was conducted retrospectively. The experimental procedures of this study were approved by the Ethical Committee of Fatih University.

High-resolution three-dimensional human brain images were recorded by a Siemens Symphony Magnetom Aera 1.5 T MR scanner (Erlangen, Germany). The image parameters included the following: 24 contiguous 5 mm sagittal slices; flip angle 90°, TE (echo time) 9.8 ms, TR (repetition time) 511 ms, field of view (FOV) 25 cm, matrix size 512 × 512, and in-plane spatial resolution of 0.5 mm × 0.5 mm.

### 2.2 Image processing

In the present study, image processing tasks were implemented for achieving three different outcomes, including measurement of cerebellar tonsil lengths, computation of 3D FD values and quantification of cerebellar WM, GM and CSF volumes. These tasks are listed in the flowchart that is illustrated in Fig. 1. To compute the FD values, first segmentation of brain tissues are required. A 3D mask image of cerebellum, which is obtained by means of a manual segmentation step, is further needed to extract the mentioned cerebellar tissues from

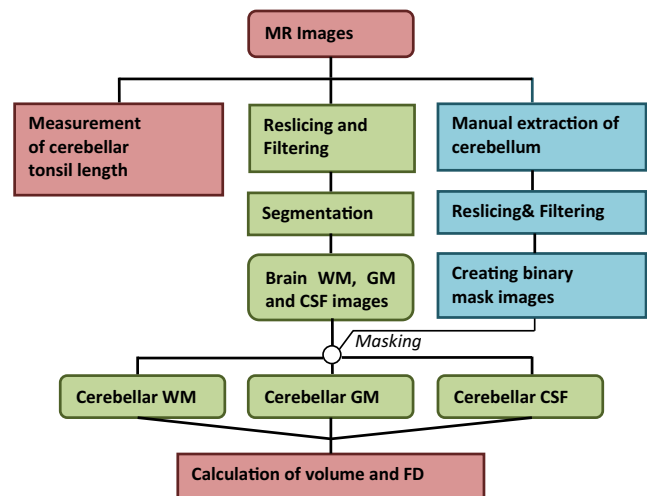


**Fig. 1** Steps of image processing

the whole image of segmented tissues. These steps are explained in the subsequent sections in detail. All image processing operations were carried out using MATLAB and a graphical user interface (GUI) application based on a MATLAB GUI development environment that was built for the facilitation of image operations.

#### 2.2.1 Measuring the length of cerebellar tonsils

The cerebellar tonsils are rounded structures that are located under the bottom parts of each cerebellar hemisphere. In this study, the extent of tonsillar herniation in each Chiari patient was measured using midline sagittal MRI slices. First, a line is drawn between the midpoints of the anterior and the posterior margins of the foramen magnum, which are defined as the basion and the opisthion, respectively. Following this, a second line is drawn from the tip of a cerebellar tonsil to the previously drawn line. The size of this second line gives the length of tonsillar herniation. This procedure is demonstrated in Fig. 2a. In addition, a midline sagittal image of a normal subject is shown in Fig. 2b for a visual comparison of cerebellar tonsil positions between an affected patient and a normal subject.

#### 2.2.2 Creating mask image of cerebellum

The segmentation of cerebellum into constituent tissue classes, including WM, GM, and CSF, was implemented in several stages as shown in Fig. 1. First, a mask image was needed to extract the mentioned tissues located at cerebellar region from the entire segmented images of brain. Therefore, MRI slices that contained the cerebellum were chosen, and the corresponding cerebellar region was separated manually from the main image by specifying its borders as shown in Fig. 3b–d. This operation was carried out under the control of an experienced radiologist. The other slices that did not include the

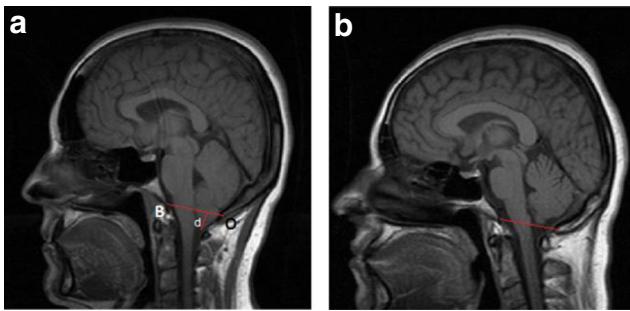


**Fig. 2** Measurement of cerebellar tonsil descent. **a** Descent of the cerebellar tonsils is measured by calculating the length between the tip of a tonsil and a line drawn between the basion (*B*) and the opisthion. **b** Position of cerebellar tonsils in a normal subject

cerebellum were accepted as background images that were set to zero intensity values only. Following this, output slices containing the regions of interest were resliced into a voxel size of  $1 \times 1 \times 1 \text{ mm}^3$  using linear interpolation. Next, each slice was filtered by 2D median filtering with a  $3 \times 3$  default kernel to improve the signal-to-noise ratio. Finally, applying a simple thresholding operation to each slice yielded 3D binary mask image. This operation involved assigning the value one to each pixel, which holds a value greater than zero.

### 2.2.3 Segmenting cerebellar tissues

This study employed functions of the SPM12 package, which is based on a MATLAB 8.2 environment, to segment the WM, GM, and CSF tissues of the brain. SPM [53] (Statistical Parametric Mapping) is a software package that was developed by the Wellcome Department of Imaging Neuroscience

at University College London, UK, for the analysis of structural and functional brain imaging data series. The segmentation procedure provided by SPM is based on a unified segmentation model that carries out tasks such as tissue segmentation, normalization, spatial registration and bias correction all in the same model [54]. In this approach, tissue classification is modeled using a mixture of Gaussians, which defines the probability density of image intensities as a number of Gaussian distributions. The prior information regarding the tissue classes is derived from tissue probability maps that are produced from a set of correctly segmented images, and the posterior probability of these classes is obtained using the Bayesian rule.

Before the segmentation procedure was started, MRI slices in DICOM format were converted into NIfTI [55] images, which is a versatile and compact format for the facilitation of brain image analysis. In the present study, default SPM atlases, which are modified versions of the ICBM Tissue Probabilistic Atlases that are available in [56], were used for all segmentation tasks. Other parameters related to segmentation were kept as defaults, including 2 Gaussians for WM, GM, and CSF tissues and 4 Gaussians for non-brain tissues, such as bone, soft tissues and background. Additionally, values of 1 and 25 mm were used for warping regularization and warp frequency cut-off, respectively. These parameters are related to deformation to be modeled and the smoothness of this warping operation applied on tissue atlases. A value of 0.0001 was used as the prior probability for any particular pattern of non-uniformity for a very light bias regularization. Moreover, a 60 mm cutoff value was set for the bias full width at half maximum (FWHM), and a value of 3 mm was used as

**Fig. 3** Manual extraction of cerebellum. **a** Montage image of sequential T1-weighted sagittal MRI slices. **b** A slice selected to perform manual border selection to separate the cerebellar region of an entire brain image is depicted in (c). **d** The extracted cerebellar region

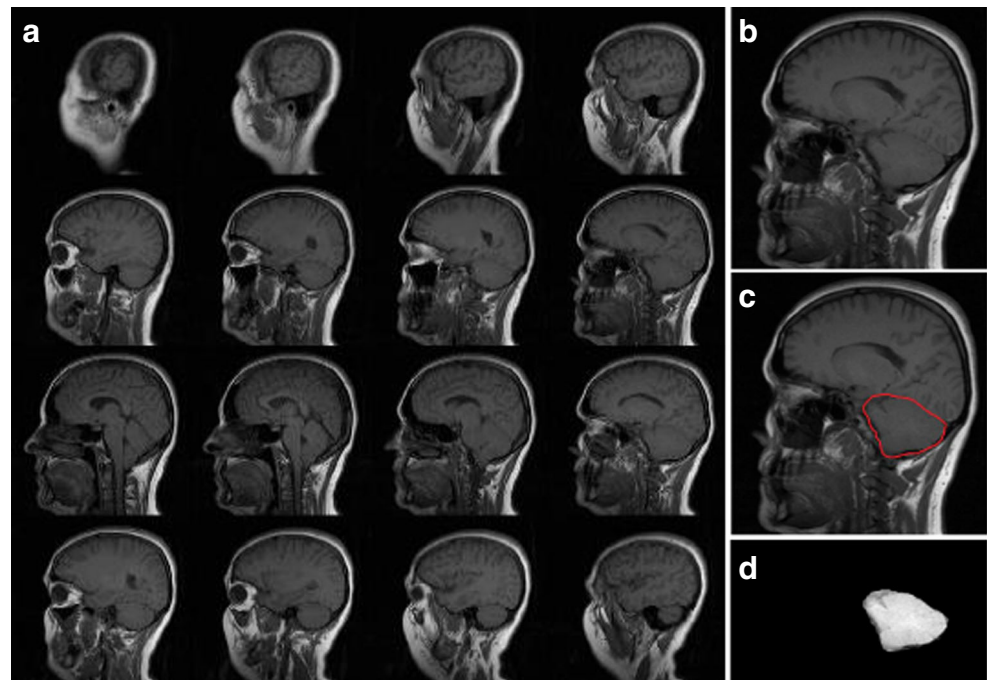
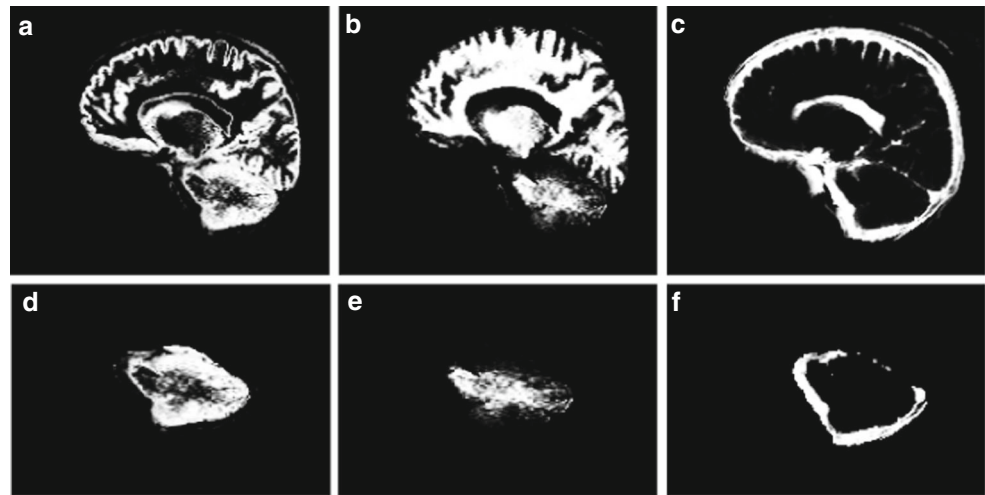


**Fig. 4** Segmentation of GM, WM, and CSF regions from MRI. **a–c** Segmented GM, WM, and CSF regions for total brain and cerebellum. **d–f** Segmented GM, WM, and CSF regions for cerebellum after applying a mask that was created using the extracted cerebellum image in Fig. 3d to the regions in (a–c)



the sampling distance. Default SPM values were kept in setting these parameters. As a result of the segmentation procedure, three NIfTI files were generated for brain WM, GM, and CSF tissues (Fig. 4a–c). Finally, the previously generated cerebellum mask file was used to produce volumetric images that contained only cerebellar WM, GM, and CSF (Fig. 4d–f). The volume of each tissue was estimated by a volumetric sum of the total number of voxels in the corresponding images.

### 2.3 3D fractal dimension computation

In the present study, a box-counting method was employed to calculate the FD values of segmented cerebellar GM, WM and CSF. This approach has been employed in many studies because of its robustness, easy implementation and applicability to objects without self-similarity, such as brain structures, which are self-similar only in specific scales [57]. The 3D box-counting method that was used in this study was an extension of a 2D approach and was developed in a MATLAB environment as custom software.

Implementation of the 3D box-counting method involves covering a corresponding volumetric image with a 3D grid and counting how many boxes hold at least one non-zero-valued pixel. This process is performed iteratively for different box size values. Figure 5a–b displays mesh objects embracing cerebellum GM and WM in 2D and 3D environments, respectively. This study was initiated using a box size of two pixels, and in each iteration, the box size value was incremented. When the box size value reached one third of the smallest dimension of the image, the iteration for counting non-empty boxes was terminated. Following this, the FD value could be estimated using the following formula [58]:

$$\ln(N_r) = \text{FD} \ln(r^{-1}) + \ln(K) \tag{1}$$

where  $r$  denotes the box size in pixels  $N_r$  is the number of boxes that contain at least one pixel value greater than zero,

FD, as the box counting dimension, denotes the complexity of the corresponding image, and  $K$  is a constant.

Because the fractals in the images of interest in the present study are not pure fractals, the selection of an appropriate box-size range is important [57]. When the size of the boxes that cover a corresponding image is too small or too large, the complexity value of that image cannot be determined properly [59]. To estimate an FD value accurately, the linear portion of the function in (1) is required. Therefore, linear regression analyses were performed on the whole data set. In these analyses, the slopes of data segments of different sizes were evaluated, and the slope of the segment that produced the highest correlation coefficient was accepted as the FD value of the corresponding image. To check the validity of our algorithm, a Menger cube ( $243 \times 243 \times 243$  in size) that was generated in MATLAB was used (Fig. 6a). According to the slope analysis that is shown in Fig. 6b, the result of the FD calculation program for the generated Menger cube is 2.7289, which is a proximate value to the theoretical FD value of 2.726833 ( $\log_{20}/\log_3$ ). Figure 10a–c displays the similar analysis for a

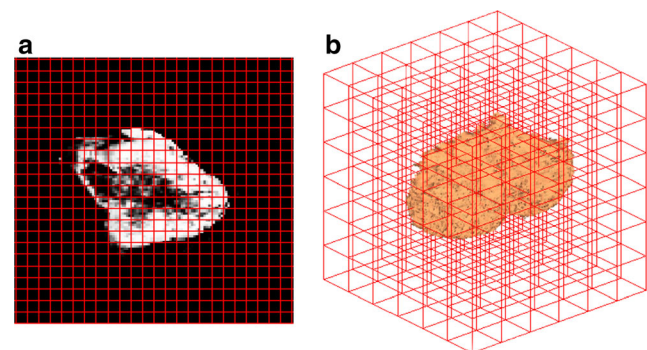


**Fig. 5** 3D FD calculation operation based on a box-counting method using segmented MRI data. Segmented images were covered by a 3D grid of boxes of size  $r$ , and the number of boxes ( $N$ ) having at least one non-zero pixel was counted in (a). Cerebellar GM image covered by a 2D grid of boxes ( $r = 5$ ). **b** Cerebellar WM image covered by a 3D grid of boxes ( $r = 20$ )

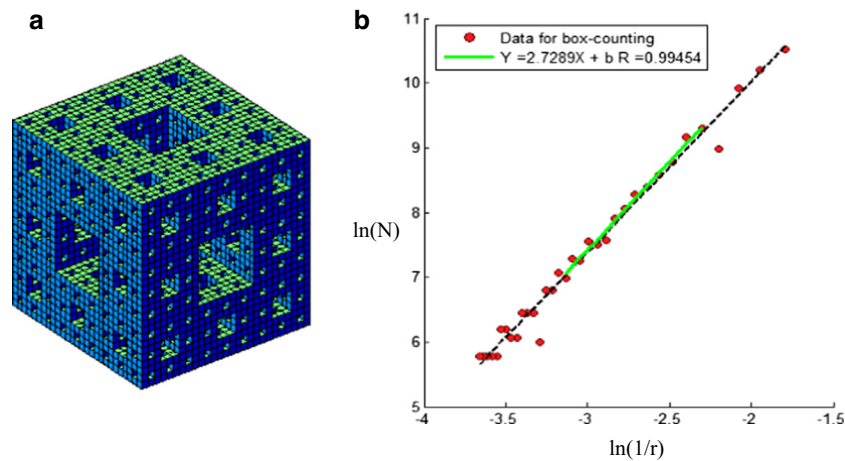


**Fig. 6** Slope analysis for determining the appropriate range of box-size for the FD estimation of a Menger-Sponge cube. **a** Menger-Sponge cube generated in four iterations. **b** Logarithmic plot of box-size ( $r$ ) and number of boxes ( $N$ ). The x-axis shows the natural logarithm of the inverse of

the box-size, and the y-axis shows the natural logarithm of the box count value. The most significant correlation was found in the regression line that was drawn between 10 and 23 pixel points

patient data. The green line in this figure represents the segment of data points that are the most significantly correlated and its slope provides the FD value of the corresponding image.

## 2.4 Statistical analysis

The differences in cerebellar WM, GM, and CSF FD values and volumes between patients with Chiari and healthy control subjects were evaluated using independent samples t-tests. The normality of the data indicating that no significant differences were found in the cerebellar features between patients and controls was checked using a Kolmogorov-Smirnov test. The correlation of cerebellar FD values with cerebellar volumes and cerebellar tonsil length was evaluated using bivariate correlation based on Pearson's method for both patient and control groups. The significance level for all results was accepted as  $p < 0.05$ . All statistical analyses were performed using SPSS version 20.0 (SPSS Inc., Chicago, Illinois).

## 3 Results

In this study, volumes and FD values of cerebellar WM, GM, and CSF were calculated and evaluated together with lengths of cerebellar tonsils (Fig. 7). These structures for the whole brain are presented in Fig. 8. The corresponding results are listed in Table 1. The mean and standard deviation values for cerebellar WM volumes of patients were found to be lower than those of controls. The difference between patients and healthy controls in terms of cerebellar WM volumes is statistically insignificant ( $p = 0.121$ ). Figure 9b shows these values for both patients and controls. On the other hand, a statistically

significant difference ( $p = 0.038$ ) was observed between cerebellar GM volumes in patients and controls (Fig. 9d). Similarly another significant difference ( $p = 0.001$ ) was found in cerebellar CSF volumes between patients and controls. The corresponding values are displayed in the box-plot presented in Fig. 9f.

Box-plot diagrams in Fig. 9a–e show FD value relationships between patients and controls. The difference in the mean values between patients and controls is statistically significant ( $p = 0.015$ ). Similar to the results from WM, higher FD values were found in cerebellar GM in controls compared to patients. However, a statistically significant difference was not found between the two groups ( $p = 0.055$ ). In CSF, a significant difference ( $p < 0.001$ ) was found between the FD values of patients and controls.

Figure 10a–c displays the correlation between the volumes of cerebellar WM, GM, and CSF and the related FD values. A significant correlation ( $R = 0.486$ ,  $p = 0.006$ ) between WM volume and WM FD value is shown in Fig. 10a. In addition, a significant correlation ( $R = 0.498$ ,  $p = 0.004$ ) was also observed between cerebellar GM FD value and volume (Fig. 10b). The correlation coefficient between cerebellar CSF volume and FD value is 0.664. This means that a highly significant correlation exists between the volumes and FD values of cerebellar CSF ( $p < 0.001$ ).

In this study, the length of cerebellar tonsil descent was also measured in the patients. The mean length of tonsillar descent is  $13 \pm 5.71$  mm (Table 1). The correlations between the FD values of cerebellar structures and the lengths of tonsillar descent are demonstrated in Fig. 11a–c for the patients. Additionally, these plots show that tonsillar descent in the patients ranges from 6 to 23 mm. Figure 11a displays the correlation between the length of the cerebellar tonsils and

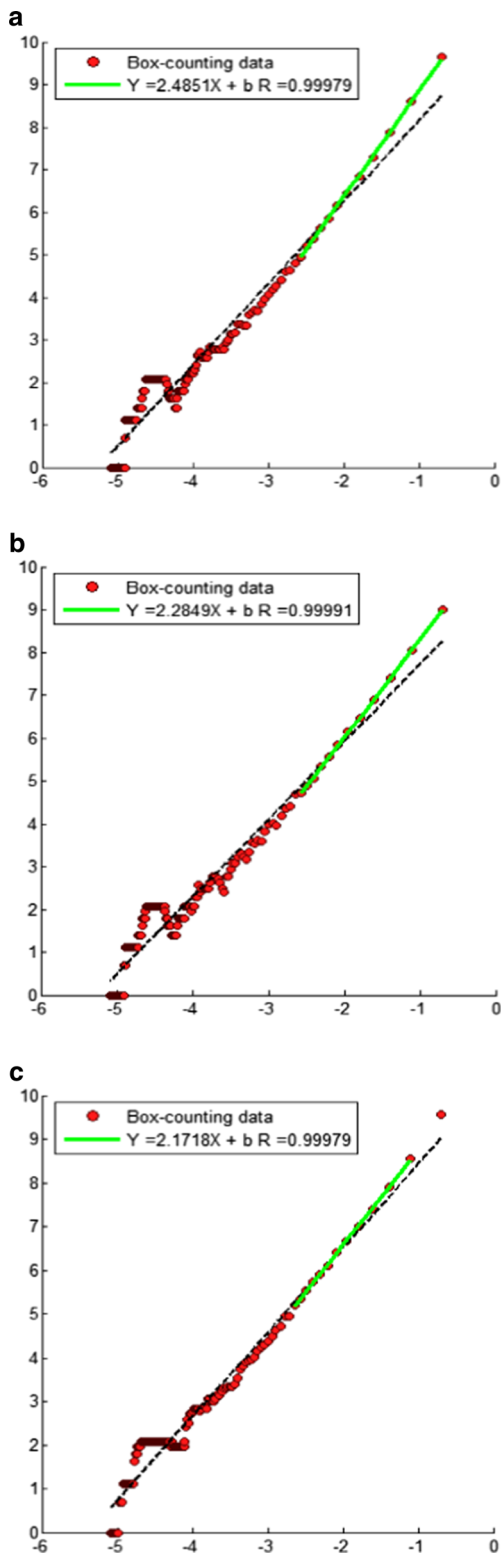


**Fig. 7** Slope analysis for a patient data. The *green line*, the slope of which gives the FD value, represents the most significant correlation between data points for segmented **a** GM, **b** WM, and **c** CSF images

the FD value of cerebellar WM. The correlation coefficient ( $R = 0.04$ ) and statistical significance ( $p = 0.889$ ) implies that the FD value of WM has a weak correlation with the descent

of cerebellar tonsils. Similarly, there is also a weak correlation between the FD value of CSF and tonsillar descent (Fig. 11c;  $R = -0.167$ ,  $p = 0.552$ ). However, Fig. 11b shows a strong correlation between the cerebellar GM FD value and tonsillar descent ( $R = -0.536$ ,  $p = 0.039$ ).

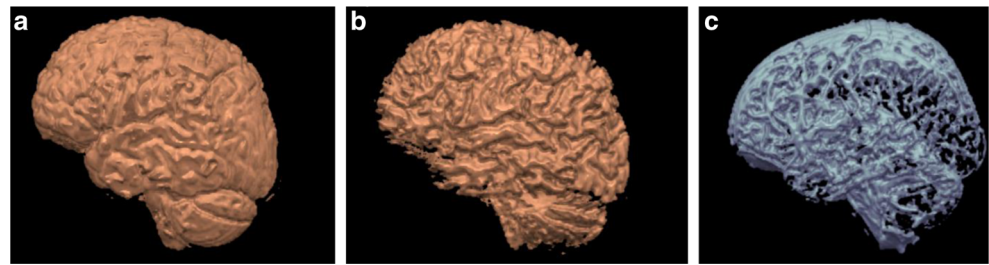
## 4 Discussion

In this study, a 3D volumetric FD analysis was carried out for morphological evaluation of constituent structures of cerebellum, including WM, GM, and surrounding CSF spaces. It was noted that the FD analysis method is useful for describing and categorizing morphological complexity in objects [60]. In light of this information, it can be stated that FD analysis may yield a more suitable description for detecting abnormalities in brain regions of interest. Therefore, our approach has additional benefits over previous work because it provides a numeric descriptor related to structural irregularities of interior regions of cerebellum.

A major result of this study was that reduced FD values for cerebellar tissues, including WM, GM, and CSF around the cerebellum, were found in patients with Chiari. It has been stated that FD is a numerical indicator of morphological complexity and that an increase in FD value may imply a more complex structure, while a lower FD value may be an indicator of a less complex structure [36]. Therefore, in line with this information, the findings in the present study suggest that the conditions of CM-I may disrupt the regularity of cerebellar WM and GM structures as well as of the CSF spaces that surround the cerebellum. From another perspective, the results are interesting in that they may be descriptive in discovering the effects of the physical conditions of Chiari disorders on the mentioned structures.

In this study, lower FD values of cerebellar GM tissue were found in patients with Chiari compared to the corresponding FD values in healthy controls. Nevertheless, this difference is not statistically significant. In some of the previous FD studies [37, 42, 43] that investigated the complexity of brain structures, findings of reduced FD values of GM tissue in brain and cerebellum were reported as being associated with degeneration and damage in GM structure. In neurodegenerative disorders such as MS and MSA, a deterioration of GM structure may be observed naturally over the course of disease. Nevertheless, a similar degeneration or volumetric change of GM in CM-I patients has not been reported to date. In a recent study [61], microstructural features of brainstem have been investigated in CM-I patients; however, GM morphology have not been mentioned particularly for those patients. Despite this, the results of the present study would help dissect the incidents involved in the formation of CM-I. It has been stated that several causes may underlie CM-I, including

**Fig. 8** Reconstructed 3D brain images. **a** GM image. **b** WM image. **c** CSF image



underdevelopment of occipital bone, compression of hind-brain in small PCF, and incidents related to para-axial mesoderm [6]. However, the exact events that cause Chiari are still unclear.

The mean FD value of cerebellar WM tissue in Chiari patients was found to be significantly lower ( $p = 0.015$ ) than the corresponding value in healthy controls. The difference in FD values of cerebellar WM between patients and controls was found to be more evident and statistically more significant in comparison with the variations in cerebellar GM FD. These lower FD values in WM may suggest that cerebellar WM tissue in patients with CM-I is more structurally irregular. No issues have been reported by previous studies related to WM morphology in CM-I. However, findings of a previous study [62] that used diffusion tensor imaging (DTI) revealed microstructural WM abnormalities in the brains of adolescents with Chiari malformation type two, which is another type of Chiari anomalies involving different conditions from CM-I type. Additionally, in a recent DTI study [61] investigating the microstructural properties of brainstem, it has been stated that the fractional anisotropy difference between CM-I patients and controls may be associated with the compressed WM tracts.

**Table 1** Demographic data of subjects and study results

	Patients	Controls	<i>p</i> value
Gender (M/F)	5/10	5/11	–
Age	39.07 ± 12.21	36.75 ± 6.04	0.504
WM volume	41.7 ± 8.01	45.77 ± 6.13	0.121
GM volume	85.6 ± 12.06	93.94 ± 9.2	0.038
CSF volume	77.53 ± 22.29	103.05 ± 17.81	0.001
WMFD value	2.20 ± 0.08	2.26 ± 0.05	0.015
GMFD value	2.45 ± 0.05	2.49 ± 0.04	0.055
CSF FD value	2.23 ± 0.08	2.34 ± 0.07	0.0003
Tonsil length	13 ± 5.71	–	–

*M/F* male/female, *WM volume* volume of cerebellar white matter ( $\text{cm}^3$ ), *GM volume* volume of cerebellar gray matter ( $\text{cm}^3$ ), *CSF volume* volume of cerebrospinal fluid in posterior cranial region surrounding the cerebellum ( $\text{cm}^3$ ), *WM FD value* FD value of cerebellar white matter, *WM FD value* FD value of cerebellar gray matter, *CSF FD value* FD value of cerebrospinal fluid surrounding the cerebellum. *Tonsil length* length of cerebellar tonsil descent (mm)

According to the results of this study, the most obvious statistical distinction between the patient and control groups ( $p < 0.001$ ) was found in the mean FD values of CSF spaces that surround the cerebellum. Similar to the findings in cerebellar WM and GM, this result may indicate irregularities and disruptions in the normal spaces of CSF around the cerebellar region. CSF issues are of particular importance in Chiari related research because the effacement of CSF spaces and obstruction of the natural flow of CSF are regarded as potential causes of the disorder and major contributors to Chiari symptomatology. Therefore, the result that these patients have lower CSF FD values is anticipated.

Along with FD values, the volumes of cerebellar WM, GM, and surrounding CSF were also calculated in this study. The CSF volume results are consistent with previous studies that found reduced CSF volumes in total cranial volume. A distinct aspect of the present study is that only the CSF spaces near the cerebellum and in the fourth ventricle were taken into account. In comparison with CSF volume values in controls, the corresponding values in patients were significantly lower ( $p = 0.001$ ). This finding is also supported by previous studies stating that CSF spaces are effaced in Chiari syndrome. Accordingly, a strong positive correlation was found between CSF volumes and FD values in both patients and controls (Fig. 10c).

An interesting result of this study is that the mean volume of cerebellar WM in Chiari patients was not found to be significantly different ( $p = 0.121$ ) from the mean volume of cerebellar WM in controls, while the mean FD values were found to be significantly different between groups. This suggests that cerebellar WM tissue size may not be affected by cerebellar compression because of small PCF. However, an irregularity in tissue complexity was still detected by FD analysis. On the other hand, a different condition was discovered for cerebellar GM. The mean FD value difference for GM between the two groups was not significant ( $p = 0.055$ ), while there was a significant difference in the mean GM volumes ( $p = 0.038$ ). This may indicate that the mechanism that results in the pathological condition of CM-I is distinct between cerebellar GM and WM tissues.

The degree of cerebellar tonsil descent below the foramen magnum was also measured in the present study. Conventionally, the length of tonsillar descent is used for the



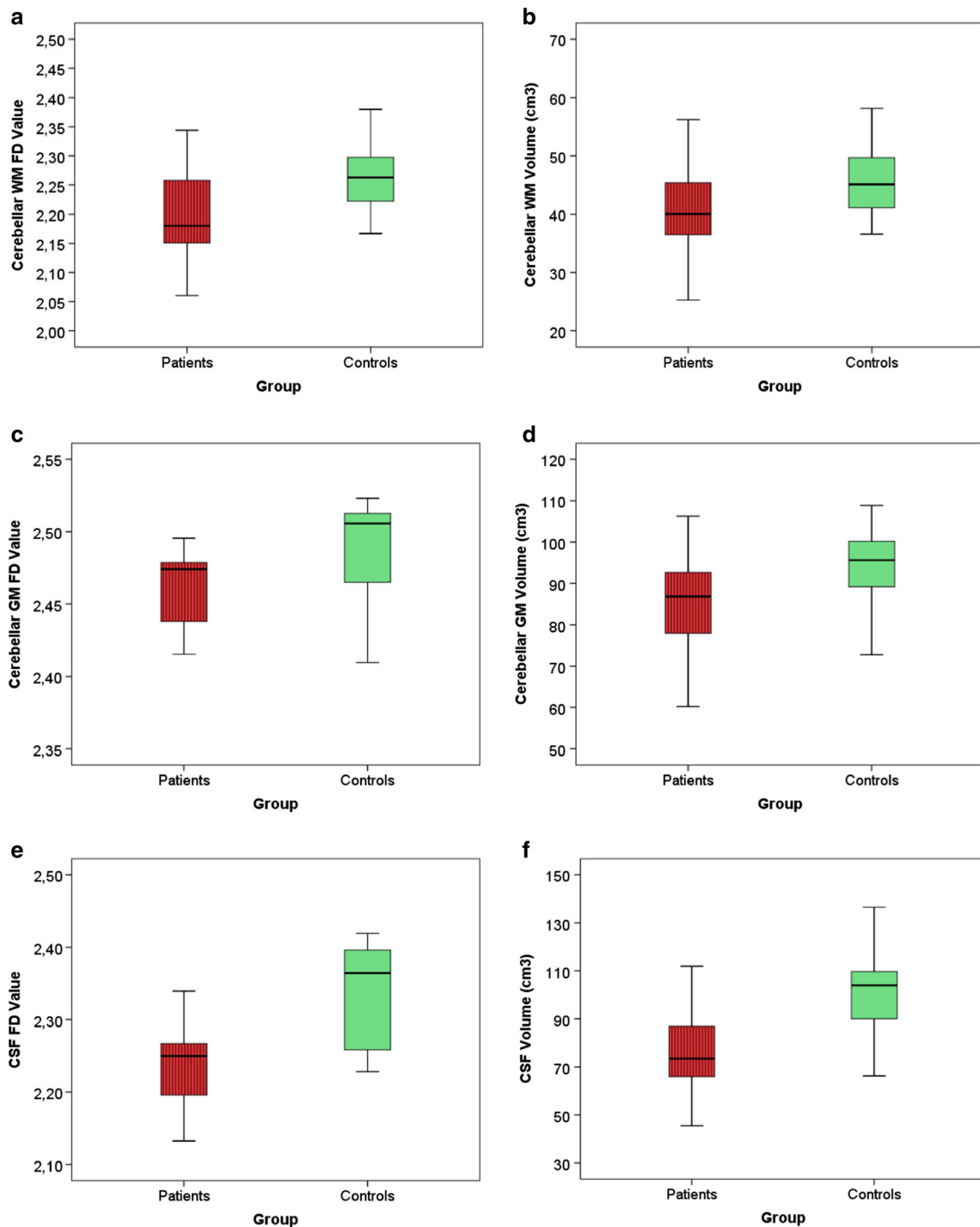


**Fig. 9** Box-plots of FD values. **a–c–e** Comparison of FD values for cerebellar WM, GM, and CSF surrounding the cerebellum between patients and controls. **b–d–f** Comparison of volumes for cerebellar WM, GM, and CSF surrounding the cerebellum between patients and controls

diagnosis and determination of the severity of the disorder. Nevertheless, in some cases, patients may be asymptomatic despite having a longer cerebellar tonsil descent, while in other cases patients may have severe symptoms even though their tonsillar descent does not match with diagnosis criteria. In the present study, no correlations were found between length of tonsillar descent and FD values of WM and CSF ( $R = 0.04$  and

$R = -0.167$ , respectively); however, a strong negative correlation was detected between GM FD values and length of tonsillar descent. These findings support the idea that cerebellar tonsil length cannot be used as a unique marker of the diagnosis or severity of CM-I disorder. Additionally, this may also indicate that WM and GM tissues are differently affected over the course of the disease.

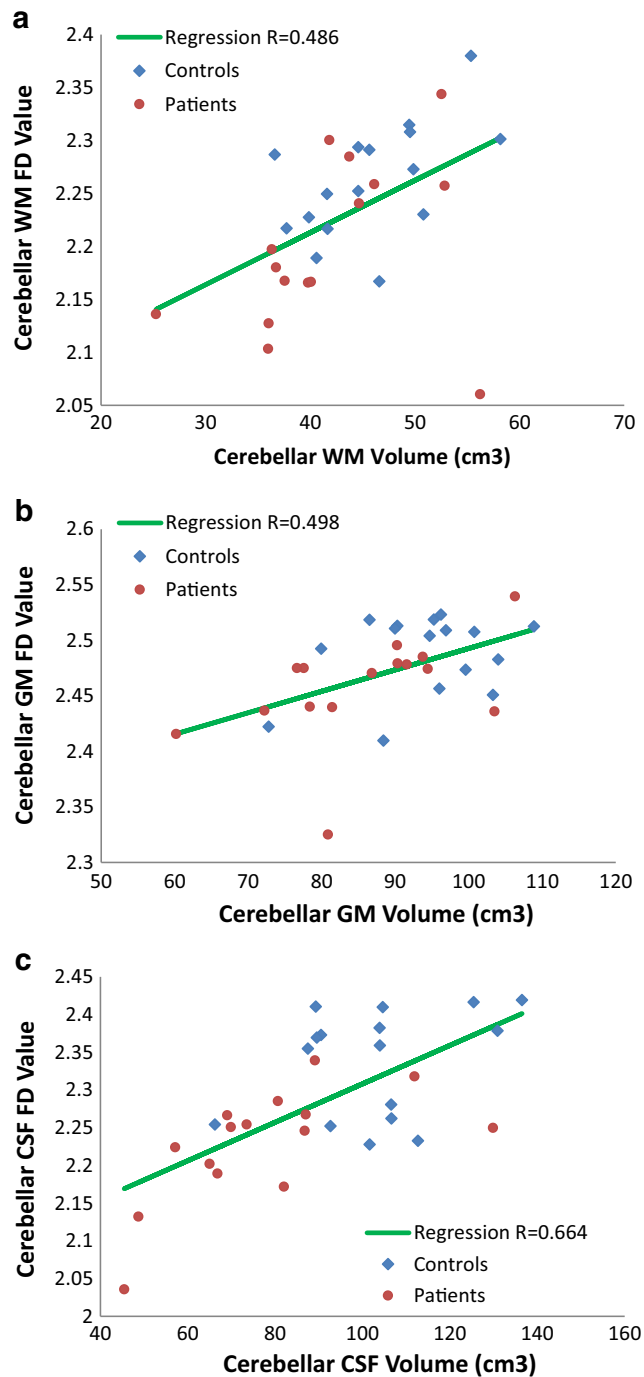


**Fig. 10** Scatter diagrams of volumetric values versus FD values. **a** Scatter plot of cerebellar WM FD and volume values. The *green regression line* indicates a significant correlation ( $R = 0.486$ ). **b** Scatter plot of cerebellar GM FD and volume values. **c** Scatter plot of CSF FD and volume values. A high correlation coefficient is exhibited by the *green regression line* for (b) and (c) ( $R = 0.498$  and  $R = 0.664$ , respectively)

The higher FD values were estimated in this study for three segmented tissues in patients compared to corresponding values in controls. However, in our previous study [50] examining the FDs of the similar cerebellar tissues segmented from

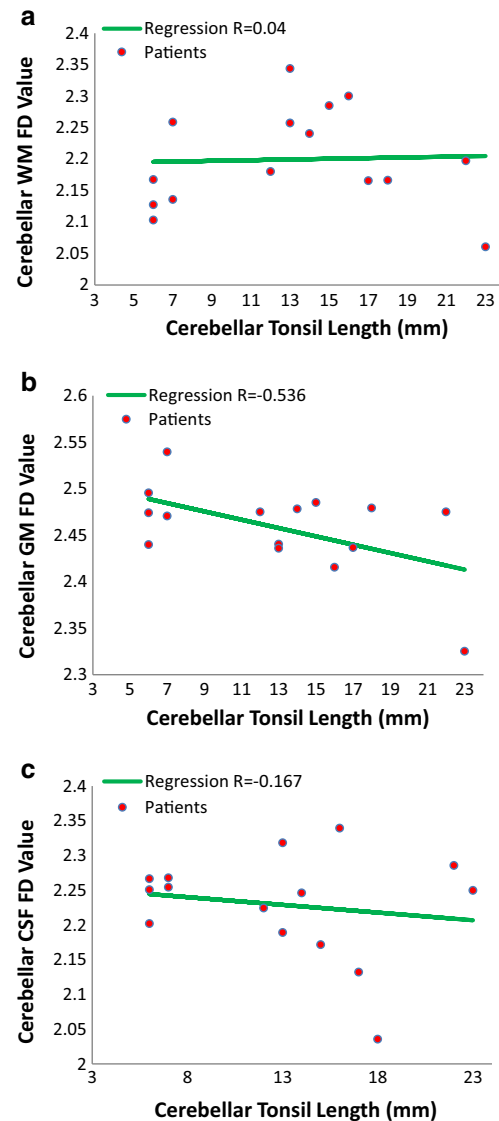


**Fig. 11** Scatter plots of FD values versus length of cerebellar tonsil descent. **a** Scatter plot of cerebellar WM FD and tonsillar descent. **b** Scatter plot of cerebellar GM FD and tonsillar descent. **c** Scatter plot of CSF FD and tonsillar descent. The *green regression lines* in **a** and **c** indicate weak correlations ( $R = 0.04$  and  $R = -0.167$ , respectively), whereas the *green line* in (b) shows a significant negative correlation ( $R = -0.536$ )

a single sagittal slice of brain, we found an increase rather than a decrease in the FDs of these tissues in CM-I patients. The analysis in the present study covered all the voxels of segmented tissues throughout cerebellum. Therefore, the results of the present study are important when the overall morphology of cerebellum is taken into account. Besides, the difference in the FD results between the two studies suggests that the complexity of tissues in several regions of cerebellum may be differently affected by the physical variations in this anomaly.

Morphological variations in brain MR images have been investigated by means of various methods such as voxel-

based morphometry (VBM) [63, 64], volumetric analysis [65], and FD analysis [35–52]. VBM method helps identifying differences in the anatomy of brain between different subject groups using structural MRI. In this technique, statistical tests are performed at each voxel in the image to compare brains and to find out and investigate the tissue atrophy. Although it is easy to use and produce reasonable results, it was reported that application of VBM may lead to errors eventually and originally it is a qualitative analysis rather than a quantitative analysis [37]. On the other hand, volumetric analysis, which is a region-of-interest (ROI)-based method to measure the volume of segmented parts of the brain, has been widely applied for examining morphological alterations in brain. In CM-I research, volumetric calculations were carried out to measure the total volume of the PCF, CSF and brain volumes in the PCF [6]. Volumetric analysis may be useful to exhibit the changes in different study groups. However, since FD analysis is based on logarithm scale, it is more sensitive to structural variations and more suitable to characterize the variability and the complexity of the tissues [37].

Employing various FD calculation methods may be another factor that affects the results. Box-counting method is the most popular way of estimating the FD for brain images and therefore it was used in the present study. A significant difference was observed in FD values for the WM and CSF, while fractal properties of GM tissues could not be discriminated successfully with this method. Alternative methods such as hands and divider, prism counting, epsilon-blanket, and hybrid methods [66, 67] have also been suggested for estimation of FD. Approaches that compute the multifractal spectrum of a signal for FD estimation such as wavelet transform based methods were mentioned in [68]. In such methods, components of a signal can be represented as an oscillating box by means of its wavelet transform, which eliminates the need for making its grid representation. Wavelet-based methods have not been implemented in brain image processing studies before and may be used to see their influence on brain image morphology analysis.

Successful and accurate implementation of the image processing operations such as noise filtering and segmentation may have considerable effects on the sensitivity and the accuracy of the FD analysis. In the present study, 2D median filtering approach was applied on each MRI slice separately as a preprocessing step. Applying the same method in a 3D manner to the volumetric MR data or employing a different method may affect the outcome of the study. In our previous study [69], the effect of using two different filtering approaches, median filtering and bilateral filtering, on the results of FD analysis on MRI data of CM-I patients and normal subjects were investigated. Our findings indicated that while GM findings were not found statistically significant ( $p = 0.051$ ) after a median filtering applied as a preprocessing, significant difference was observed ( $p = 0.007$ ) in bilateral filtering case.

Additionally, accurate segmentation of the brain tissues may also affect the sensitivity of the findings of this study. This study kept default values for SPM parameters in the segmentation of the brain tissues. Trying different values for these parameters may also change the final results.

Several factors limited an effective evaluation of the findings in the present study. The foremost limitation was the relatively small number of subjects in each of the groups. These analyses should be replicated on larger populations to prove their usefulness and to improve the significance of our results. Furthermore, a lack of reference in the literature on the effects of CM-I pathology on WM and GM tissues impeded our ability to make comparisons and more proper inferences. In addition, already existing MRI data were used in this study. For this reason, as the symptoms of the included patients could not be obtained, we were unable to correlate our results with them.

In future work, this study may be extended to involve whole brain structure. Additionally, the results may be evaluated together with the symptoms of patients to understand the effects of morphological change on the symptomatology of the Chiari anomaly. Moreover, further studies must be carried out to investigate whether complexity variances in the sub-regions of CM-I patients are related to some set of common symptoms that are observed in other neurological disorders. Finally, different automated segmentation methods as alternatives to SPM segmentation approach may be employed to investigate the accuracy and sensitivity of different approaches in brain tissue classification of CM-I MRI data.

In conclusion, a 3D FD method was carried out to detect and evaluate morphological differences between CM-I patients and healthy subjects. We report that 3D nonlinear MRI analysis indicates significant differences between patients with Chiari and healthy control subjects. According to the findings of this study, patients with CM-I have reduced values of FD in cerebellar WM and GM tissues and in CSF surrounding the cerebellum, although the reduction was statistically significant for WM and CSF only. This may be a useful indicator to distinguish between asymptomatic and symptomatic CM-I patients.

**Acknowledgements** This research was supported by the Fatih University Research and Development Management Office under project number P58011501\_B.

## References

1. Cai C, Oakes WJ (1997) Hindbrain herniation syndromes: the Chiari malformations (I and II). *Semin Pediatr Neurol* 4(3):179–191

2. Bejjani GK (2001) Definition of the adult Chiari malformation: a brief historical overview. *Neurosurg Focus* 11
3. Elster AD, Chen MYM (1992) Chiari I malformations: clinical and radiologic reappraisal. *Radiology* 183:347–353
4. Osborn AG (1994) Disorders of neural tube closure. In: *Diagnostic Neuroradiology* (ed) 2. St. Louis Mosby, p 15
5. Chiari H (1891) Über Veränderungen des Kleinhirns in folge von Hydrocephalie des Grosshirns (in German). *Dtsch med Wschr* 17: 1172–1175
6. Milhorat TH, Chou MW, Trinidad EM, Kula RW, Mandell M, Wolpert C, Speer MC (1999) Chiari I malformation redefined: clinical and radiographic findings for 364 symptomatic patients. *Congress of Neurological Surgeons* 44(5):1005–1017
7. Milhorat TH, Nishikawa M, Kula RW, Dlugacz YD (2010) Mechanisms of cerebellar tonsil herniation in patients with Chiari malformations as guide to clinical management. *Acta Neurochir (Wien)* 152(7):1117–1127
8. Badie B, Mendoza D, Batzdorf U (1995) Posterior fossa volume and response to suboccipital decompression with Chiari I malformation. *Neurosurgery* 37:214–218
9. Nishikawa M, Sakamoto H, Hakuba A, Nakanishi N, Inoue Y (1997) Pathogenesis of Chiari malformation: a morphometric study of the posterior cranial fossa. *J Neurosurg* 86:40–47
10. Nyland H, Krogness KG (1978) Size of posterior fossa in Chiari type 1 malformation in adults. *Acta Neurochir* 40:233–242
11. Stovner LJ, Bergan U, Nilsen G, Sjaastad O (1993) Posterior cranial fossa dimensions in the Chiari I malformation: relation to pathogenesis and clinical presentation. *Neuroradiology* 35:113–118
12. Milhorat TH, Chou MW, Trinidad EM, Kula RW, Mandell M, Wolpert C, Speer MC (1999) Chiari I malformation redefined: clinical and radiographic findings for 364 symptomatic patients. *Neurosurgery* 44(5):1005–1017
13. Novegno F, Caldarelli M, Massa A, Chieffo D, Massimi L, Pettorini B, Tamburrini G, Di Rocco C (2008) The natural history of the Chiari type I anomaly. *J Neurosurg Pediatr* 2:179–187
14. Talal AA, el-Shmami OM (1997) Chiari Malformation Type I: A New MRI Classification. *Magn Reson Imaging* 15(4):397–403
15. Carlson MD, Muraszko MK (2003) Chiari I malformation with syrinx. *Pediatr Neurol* 29(2):167–169
16. Yassari R, Frim D (2004) Evaluation and management of the Chiari malformation type 1 for the primary care pediatrician. *Pediatr Clin N Am* 51(2):477–490
17. Lam B, Ryan CF (2000) Arnold-Chiari malformation presenting as sleep apnea syndrome. *Sleep med* 1:139–144
18. Kitamura T, Miyazaki S, Kadotani H, Kanemura T, Okawa M, Tanaka T, Komada I, Hatano T, Suzuki H (2014) Type I Chiari malformation presenting central sleep apnea. *Auris Nasus Larynx* 41(2):222–224
19. Choi SS, Tran LP, Zalzal GH (1999) Airway abnormalities in patients with Arnold-Chiari malformation. *Otolaryngol Head Neck Surg* 121(6):720–724
20. Holinger PC, Holinger LD, Reichert TJ et al (1978) Respiratory obstruction and apnea in infants with bilateral abductor vocal cord paralysis, meningocele, hydrocephalus, and Arnold-Chiari malformation. *J Pediatr* 92:368–373
21. Pieh C, Gottlob I (2000) Arnold-Chiari malformation and nystagmus of skew. *J Neurol Neurosurg Psychiatry* 69:124–126
22. Staudt MD (2013) Gait disturbances and seizure-like episodes in a patient with a Chiari malformation. *UWOMJ. Summer Supplement Issue S1* 81:11–12
23. Meadows J, Kraut M, Guarnieri M, Haroun RI, Carson BS (2000) Asymptomatic Chiari type I malformations identified on magnetic resonance imaging. *J Neurosurg* 92:920–926
24. Speer MC, Enterline DS, Mehlretter L, Hammock P, Joseph J, Dickerson M et al (2003) Chiari type I malformation with or without syringomyelia: prevalence and genetics. *J Genet Counsel* 12:297–311
25. Cama A, Tortori-Donati P, Piatelli GL et al (1995) Chiari complex in children—neuroradiological diagnosis, neurosurgical treatment and proposal of a new classification (312 cases). *Eur J Pediatr Surg* (suppl 1), 35–8.
26. Choudhury PR, Sarda P, Baruah P, Singh S (2013) A magnetic resonance imaging study of congenital Chiari malformations. *OA Case Reports* 2(8):73
27. Khan AA, Bhatti SN, Khan G, Ahmed E, Aurangzeb A, Ali A, Khan A, Afzal S (2010) Clinical and radiological findings in Arnold Chiari malformation. *J Ayub Med Coll Abbottabad* 22(2): 75–78
28. Houghton VM, Iskandar BJ (2006) Measuring CSF flow in Chiari I malformations. *Neuroradiol J* 19:427–432
29. Navarro R, Olavarria G, Seshadri R, Gonzales-Portillo G, McLone DG, Tomita T (2004) Surgical results of posterior fossa decompression for patients with Chiari I malformation. *Childs Nerv Syst* 20(5):349–356
30. Brugieres P, Idy-Peretti I, Iffenecker C et al (2000) CSF flow measurement in syringomyelia. *AJNR Am J Neuroradiol* 21(10):1785–1792
31. Chang HS, Nakagawa H (2003) Hypothesis on the pathophysiology of syringomyelia based on simulation of cerebrospinal fluid dynamics. *J Neurol Neurosurg Psychiatry* 74(3):344–347
32. Clatterbuck RE, Sapos EP (1997) The efficient calculation of neurosurgically relevant volumes from computed tomographic scans using Cavalieri's direct estimator. *Neurosurgery* 40:339–343
33. Aydin S, Hanimoglu H, Tanriverdi T, Yentur E, Kaynar MY (2005) Chiari type I malformations in adults: a morphometric analysis of the posterior cranial fossa. *Surg Neurol* 64(3):237–241
34. Clarke EC, Fletcher DF, Stoodley MA, Bilston LE (2011) Computational fluid dynamics modelling of cerebrospinal fluid pressure in Chiari malformation and syringomyelia. *J Biomech* 46:1801–1809
35. Ha TH, Yoon U, Lee KJ, Shin YW, Lee JM, Kim IY, Ha KS, Kim SI, Kwon JS (2005) Fractal dimension of cerebral cortical surface in schizophrenia and obsessive-compulsive disorder. *Neurosci Lett* 384:172–176
36. Esteban FJ, Sepulcre J, de Mendizábal NV, Goñi J, Navas J, de Miras JR, Bejarano B, Masdeu JC, Villoslada P (2007) Fractal dimension and white matter changes in multiple sclerosis. *Neuro Image* 36:543–549
37. Wu YT, Shyu KK, Jao CW, Wang ZY, Soong BW, Wu HM, Wang PS (2010) Fractal dimension analysis for quantifying cerebellar morphological change of multiple system atrophy of the cerebellar type (MSA-C). *NeuroImage* 49:539–551
38. Shan ZY, Liu JZ, Glassa JO, Gajjar A, Lid CS, Reddick WE (2006) Quantitative morphologic evaluation of white matter in survivors of childhood medulloblastoma. *Magn Reson Imaging* 24: 1015–1022
39. Free SL, Sisodiya SM, Cook MJ, Fish DR, Shorvon SD (1996) Three dimensional fractal analysis of the white matter surface from magnetic resonance images of the human brain. *Cereb Cortex* 6: 830–836
40. Liu JZ, Zhang LD, Yue GH (2003) Fractal dimension in human cerebellum measured by magnetic resonance imaging. *Biophys J* 85:4041–4046
41. Lee JM, Yoon U, Kim JJ, Kim IY, Lee DS, Kwon JS, Kim SI (2004) Analysis of the hemispheric asymmetry using fractal dimension of a skeletonized cerebral surface. *IEEE Trans Biomedical Eng* 51: 1494–1498
42. Esteban FJ, Sepulcre J, de Miras JR, Navas J, de Mendizábal NV, Goñi J, Quesada JM, Bejarano B, Villoslada P (2009) Fractal dimension analysis of grey matter in multiple sclerosis. *J Neuro Sci* 282:67–71

43. Sandu AL, Rasmussen IA, Lundervold A, Frank Kreuder F, Neckelmann G, Hugdahl K, Specht K (2008) Fractal dimension analysis of MR images reveals grey matter structure irregularities in schizophrenia. *Comput med Imaging Graph* 32:150–158
44. Zhao G, Denisova K, Sehatpour P, Long J, Gui W, Qiao J et al (2016) Fractal dimension analysis of subcortical gray matter structures in schizophrenia. *PLoS One* 11(5):e0155415. doi:10.1371/journal.pone.0155415
45. Pereira D, Zambrano C, Martin-Landrove M (2000) Evaluation of malignancy in tumors of the central nervous system using fractal dimension. *Eng. Med. Biol. Soc. proc. of the 22nd Annu. Intl. Conference of the IEEE* 3:1775–1778
46. Zook JM, Iftekharuddin KM (2005) Statistical analysis of fractal-based brain tumor detection algorithms. *Magn Reson Imaging* 23:671–678
47. Takahashi T, Murata T, Omori M, Kosaka H, Takahashi K, Yonekura Y, Wada Y (2004) Quantitative evaluation of age related white matter micro structural changes on MRI by multifractal analysis. *J Neurol Sci* 225:33–37
48. Cook MJ (1995) Fractal description of cerebral cortical patterns in frontal-lobe epilepsy. *Eur Neurol* 35(6):327–335
49. King RD, George AT, Jeon T, Hynan LS, Youn TS, Kennedy DN, Dickerson B (2009) Characterization of atrophic changes in the cerebral cortex using fractal dimensional analysis. *Brain Imaging Behav* 3:154–166
50. Zhang L, Butler AJ, Sun CK, Sahgal V, Wittenberg GF, Yue GH (2008) Fractal dimension assessment of brain white matter structural complexity post stroke in relation to upper-extremity motor function. *Brain res* 1228:229–240
51. Zhang L, Yue GH (2016) Fractal dimension studies of the brain shape in aging and neurodegenerative diseases. In *Book: the Fractal Geometry of the Brain*, pp:213–232. doi:10.1007/978-1-4939-3995-4\_14
52. Akar E, Kara S, Akdemir H, Kırış A (2015) Fractal dimension analysis of cerebellum in Chiari malformation type I. *Comput Biol med.* doi:10.1016/j.compbiomed.2015.06.024
53. Ashburner J, Friston KJ, Poline J et al (1995) Spatial registration and normalization of images. *Hum Brain Mapp* 2:165–189
54. Ashburner J, Friston KJ (2005) Unified segmentation. *NeuroImage* 26(3):839–851
55. NifTI (2015) Neuroimaging Informatics Technology Initiative <http://nifti.nimh.nih.gov/>
56. LONI (2015) Laboratory of Neuro Imaging, ICBM Probabilistic Atlases [http://www.loni.usc.edu/ICBM/Downloads/Downloads\\_ICBMprobabilistic.shtml](http://www.loni.usc.edu/ICBM/Downloads/Downloads_ICBMprobabilistic.shtml)
57. Zhang L, Liu JZ, Dean D, Sahgal V, Yue GH (2006) A three-dimensional fractal analysis method for quantifying white matter structure in human brain. *J Neurosci Methods* 150:242–253
58. Mandelbrot BB (1983) *The fractal geometry of nature*. W.H. Freeman, New York
59. NeZadal M, Zmeskal O, Buchniecek M (2001) The box-counting: critical study. In: *Proceedings of the Fourth Conference on Prediction, Synergetic and More* 2001:18 (ISBN 80-7318-030-8).
60. Fernández E, Jelinek HF (2001) Use of fractal theory in neuroscience: methods, advantages, and potential problems. *Methods* 24(4):309–321
61. Krishna V, Sammartino F, Yee P, Mikulis D, Walker M, Elias G, Hodaie M (2016) Diffusion tensor imaging assessment of microstructural brainstem integrity in Chiari malformation type I. *J Neurosurg* 125(5):1112–1119
62. Ou X, Glasier CM, Snow JH (2011) Diffusion tensor imaging evaluation of white matter in adolescents with myelomeningocele and Chiari II malformation. *Pediatr Radiol* 41(11):1407–1415. doi:10.1007/s00247-011-2180-6
63. Lukas C, Schöls L, Bellenberg B, Rüb U, Przutek H, Schmid G, Koster O, Suchan B (2006) Dissociation of grey and white matter reduction in spinocerebellar ataxia type 3 and 6: a pixel-based morphometry study. *Neurosci Lett* 408:230–235
64. Smith CD, Chebrolu H, Wekstein DR, Schmitt FA, Markesbery WR (2007) Age and gender effects on human brain anatomy: a pixel-based morphometric study in healthy elderly. *Neurobiol Aging* 28:1075–1087
65. Bürk K, Globas C, Wahl T, Bühring U, Diety K, Yühlke C, Luft A, Schuly JB, Voigt K, Dichgans J (2004) MRI-based volumetric differentiation of sporadic cerebellar ataxia. *Brain* 127:175–181
66. Napolitano A, Ungania S, Cannata V (2012) Fractal dimension estimation methods for biomedical images, MATLAB-A fundamental tool for scientific computing and engineering applications-volume 3, prof. Vasilios Katsikis (Ed.), InTech, DOI:10.5772/48760.
67. Annadhason A (2012) Methods of fractal dimension computation. *International Journal of Computer Science and Information Technology & Security (IJCSITS)* ISSN: 2249–9555 2(1):166–169
68. Lopes R, Betrouni N (2009) Fractal and multifractal analysis. *Med Image Anal* 13:634–649
69. Akar E, Kara S, Akdemir H, Kırış A (2017) Fractal analysis of MR images in patients with chiari malformation: the importance of pre-processing. *Biomedical Signal Processing and Control* 31:63–70



**Engin Akar** graduated from the department of computer engineering at Marmara University, İstanbul, Turkey, in 2004. He received the M.Sc. degree in computer engineering from Marmara University, in 2013, and the Ph.D. degree in biomedical engineering from Fatih University, İstanbul, in 2016. His research interests include biomedical image processing and hybrid evolutionary algorithms.



**Sadık Kara** received the Bachelors degree in the Department of Electronics Engineering from Erciyes University, Kayseri, Turkey, in 1988 and M.Sc and the Ph.D. degrees in Electronics Engineering, in 1991 and 1995, respectively. In 1995, he started to work as an assistant professor in the Department of Electronics Engineering in Erciyes University, where he became an associate professor in 2000, and a professor in 2006 in the field of Bioelectronics. His research interests include biomedical signal and image processing,

biomechanics and biomaterials, health informatics, telemedicine and medical instrumentation.



**Hidayet Akdemir** is a Professor of Neurosurgery and currently working as the head of Neurosurgery Department in Medicana International Hospital, İstanbul.



**Adem Kırış** is a Professor of radiology and currently working as an instructor in faculty of Medicine at Kafkas University.